AGU PUBLICATIONS

Water Resources Research

RESEARCH ARTICLE
10.1002/2013WR014459

Key Points:
- High-resolution fracture map is used to examine non-Fickian transport
- The degree of non-Fickian transport is proportional to fracture heterogeneity
- CTRW transport velocity can be predicted based on mean flow velocity

Correspondence to:
L. Wang,
wanglichun@utexas.edu

Citation:
Wang, L., and M. B. Cardenas (2013), Non-Fickian transport through two-dimensional rough fractures: Assessment and prediction, *Water Resour. Res.*, *50*, doi:10.1002/2013WR014459.

Received 22 JULY 2013
Accepted 3 JAN 2014
Accepted article online 8 JAN 2014

Non-Fickian transport through two-dimensional rough fractures: Assessment and prediction

Lichun Wang[1] and M. Bayani Cardenas[1]

[1]Department of Geological Sciences, University of Texas at Austin, Austin, Texas, USA

Abstract Non-Fickian transport ubiquitously occurs across all scales within fractured geological media. Detailed characterization of non-Fickian transport through single fractures is thus critical for predicting the fate of solutes and other fluid-borne entities through fractured media. Our direct numerical simulations of solute transport through two-dimensional rough-walled fractures showed early arrival and heavy tailing in breakthrough curves (BTCs), which are salient characteristics of non-Fickian transport. Analyses for dispersion coefficients (D_{ADE}) using the standard advection-dispersion equation (ADE) led to errors which increased linearly with fracture heterogeneity. Estimated Taylor dispersion coefficients deviated from estimated D_{ADE} even at higher Peclet numbers. Alternatively, we used continuous time random walk (CTRW) model with truncated power law transition rate probability to characterize the non-Fickian transport. CTRW modeling markedly and consistently improved fits to the BTCs relative to those fitted with ADE solutions. The degree of deviation of transport from Fickian to non-Fickian is captured by the parameter β of the truncated power law. We found that β is proportional to fracture heterogeneity. We also found that the CTRW transport velocity can be predicted based on the flow velocity. Along with the ability to predict β, this is a major step toward prediction of transport through CTRW using measurable physical properties.

1. Introduction

Fractures occur ubiquitously in geological formations due to tectonic processes. Prediction of conservative and reactive contaminant transport through fractured reservoirs is important for both environmental and engineering problems and natural geophysical phenomena [*Berkowitz*, 2002]. To date, detailed characterization of complex fracture networks remains an open problem [*Neuman*, 2005]. Thus, numerous efforts have been focused on the backbone of network models: discrete rough-walled fractures [e.g., *Cardenas et al*., 2007, 2009; *Keller et al*., 1995, 1999]. Nonetheless, large-scale models typically use so-called discrete fracture networks (DFNs) [*Berkowitz and Scher*, 1997; *Cvetkovic et al*., 2004] which tend to conceptualize the discrete fractures as parallel plates [*Maloszewski and Zuber*, 1990; *Sudicky and Frind*, 1982], which in turn is the simplest model for single fractures. Therefore, a solid basis for solute transport theory for single fractures is critical even for continuum models.

Solute transport is usually assumed to follow Fickian behavior where the dispersion coefficient is spatially and temporally constant. This is based on the assumption that geological formations of interest are statistically homogeneous and stationary, where the traditional advection-dispersion equation (ADE) holds true. *Roux et al*. [1998] explained that variation in the velocity field due to geometric properties (i.e., roughness) will lead to different dominant Fickian solute transport mechanisms through rough-walled 3-D fractures. These mechanisms are molecular diffusion, Taylor dispersion [*Aris*, 1956; *Taylor*, 1953], and macrodispersion [*Gelhar and Axness*, 1983; *Keller et al*., 1995, 1999], whose relative relevance is quantified through the dimensionless Peclet number (*Pe*) defined by:

$$Pe = \frac{\langle u \rangle \langle b \rangle}{D_m} \tag{1}$$

where $\langle u \rangle$ is the average or bulk velocity, b is the apparent aperture (the height difference between top and bottom fracture surfaces) with arithmetic mean aperture $\langle b \rangle$, and D_m is the molecular diffusion coefficient. Following *Roux et al*.'s [1998] work, *Detwiler et al*. [2000] proposed that the effective dispersion coefficient (D) of rough-walled fractures is the sum of the three mixing and spreading mechanisms:

$$D = \tau D_m + D_{\text{macro}} + D_{\text{Taylor}} \quad (2)$$

where τ is tortuosity, D_{macro} is the macrodispersion coefficient, and D_{Taylor} is the Taylor dispersion coefficient. The dominance of each term in equation (2) increases in the order they are presented from left to right with increasing *Pe*: molecular diffusion dominates at the lowest *Pe* (10^{-3} to 10^{-1}), followed by macrodispersion at intermediate *Pe* (10^{-1} to 10^{3}), and then Taylor dispersion dominates at higher *Pe* ($>10^{3}$) [*Detwiler et al*., 2000].

However, the extensive application and validation of Fickian transport theory remains a challenge since heterogeneity of geological formations occurs at all scales [*Berkowitz et al*., 2006]. Moreover, dispersive processes have been observed to increase with travel distance [*Gelhar et al*., 1992]. In fact, both laboratory and field experiments have shown fast breakthrough, multimodal behavior, and long tails in breakthrough curves of solutes transported through porous [*Silliman and Simpson*, 1987] and fractured media [*Becker and Shapiro*, 2000]. Transport behavior such as scale-dependent spreading, early arrivals, and long tails are often described as non-Fickian or anomalous transport. Fitting non-Fickian breakthrough curves (BTCs) observed in single fractures with solutions to the standard ADE shows persistent errors [*Bauget and Fourar*, 2008; *Jiménez-Hornero et al*., 2005]. Thus, there is a continuing need for further fundamental understanding and analysis of non-Fickian transport in order to better predict the fate of solutes through rough-walled fractures.

Non-Fickian transport has been broadly documented in rough-walled fractures. Enhancement of mixing and spreading of solutes purely due to variability in advective transport through fractures would lead to non-Fickian transport [*Becker and Shapiro*, 2000]. Additionally, non-Fickian transport could possibly be interpreted in terms of diffusion into and out from immobile zones [*Chen et al*., 2010], fracture skins [*Robinson et al*., 1998], and the rock matrix [*Zhou et al*., 2006], channeling [*Tsang*, 1984; *Tsang and Tsang*, 1989], as well as formation of eddies within the fracture [*Cardenas et al*., 2007]. Another explanation is that the time and length scales over which transport occurs have not reached its asymptotic threshold [*Wang et al*., 2012].

Non-Fickian transport can be mathematically characterized through different transport models including: ADE with dynamic dispersion coefficient [*Wang et al*., 2012], mobile-immobile domains [*Qian et al*., 2011], equivalent-stratified medium [*Bauget and Fourar*, 2008; *Nowamooz et al*., 2013], continuous time random walk (CTRW) [*Berkowitz et al*., 2006], fractional advection-dispersion [*Zhou et al*., 2006], and multirate mass transfer [*Haggerty*, 2013; *Wang et al*., 2005]. The descriptions of these models were recently summarized by *Neuman and Tartakovsky* [2009]. However, CTRW has been shown to better reproduce BTCs than the equivalent-stratified medium approach [*Nowamooz et al*., 2013]. Additionally, *Berkowitz et al*. [2006] suggested that mobile-immobile domain models, fractional ADE, and multirate mass transfer models represent special classes of CTRW. Therefore, for now, we focus our study on the CTRW framework.

The CTRW framework is capable of capturing Fickian and non-Fickian transport induced by unresolved heterogeneities. It resembles the ADE after inverse Laplace transformation of the generalized master equation by having both advective and dispersive terms, but additionally the contribution of local scale processes on non-Fickian transport is encapsulated by a memory function [*Berkowitz et al*., 2006; *Cortis et al*., 2004; *Margolin and Berkowitz*, 2004]. Like the ADE, the CTRW assumes stationary statistical properties in spite of its application to heterogeneous media [*Berkowitz et al*., 2006]. The successful applications of CTRW for characterizing BTCs showing non-Fickian transport are extensive. Examples include transport through heterogeneous porous media [*Cortis et al*., 2004; *Dentz et al*., 2004], "homogeneous" sand and soil columns [*Cortis and Berkowitz*, 2004], single fractures [*Bauget and Fourar*, 2008; *Jiménez-Hornero et al*., 2005], and fracture networks [*Berkowitz and Scher*, 1997, 1998].

The degree of deviation of transport to non-Fickian from Fickian can be captured by the value of β, a parameter in the truncated power law (TPL) model within the context of the CTRW framework. Three regimes of transport are classified based on β [*Nowamooz et al*., 2013]: (1) most anomalous transport where both transport velocity and dispersion coefficient scale as power laws with time when $0 < \beta < 1$; (2) moderate anomalous transport where transport velocity is constant but where dispersion coefficient still scales following a power law when $1 < \beta < 2$; (3) Fickian transport where both transport velocity and dispersion coefficient are constant when $\beta > 2$ and when the TPL-CTRW model is reduced to the ADE.

Several studies have applied the CTRW for interpretation of non-Fickian transport through single fractures [*Bauget and Fourar*, 2008; *Jiménez-Hornero et al*., 2005; *Nowamooz et al*., 2013]. One recent study has qualitatively related β to the heterogeneity of fractures [*Bauget and Fourar*, 2008]. However, the quantitative connection between these properties remains unclear, thus limiting the broad application of the CTRW for prediction of transport. In the case of 2-D fractures, heterogeneity is represented by $\sigma_b/\langle b\rangle$, where σ_b is standard deviation of apparent aperture field. In this study, we attempt to quantify the inherent relationship between heterogeneity and β which in turn provides a robust upscaling approach. Since both heterogeneity and anisotropy of fractures influence the dispersive processes [*Zheng et al*., 2009], and since this study is focused on the non-Fickian behavior induced by heterogeneity, we limit our study to two-dimensional (2-D) vertical plane high-resolution fractures instead of three-dimensional (3-D) fractures to circumvent anisotropy effects and due to computational limitations. Furthermore, for 3-D cases, the fluid would flow through the most conductive paths (i.e., high aperture regions) and around the low aperture regions. Additionally, the resultant out-of-vertical-plane velocity variations might lead to macrodispersion. However, fluid flow through 2-D models where the fluid is forced to flow through both high and low aperture regions is fundamentally different from the 3-D case. Thus, for our 2-D studies, out-of-plane velocity variation is neglected and in-plane velocity variation across the aperture is the dominant factor that drives solute dispersion. Moreover, molecular diffusion is negligible compared to Taylor dispersion in the 2-D models; this allows for one-to-one comparison to 2-D transport models which are ideal for a first-order test of the Taylor dispersion theory. This study enables us to accurately characterize non-Fickian transport caused by fracture heterogeneity through 2-D rough-walled systems. The major contributions here relative to previous work are as follows: (1) testing the validity of and quantifying the associated errors of the Taylor dispersion theory for characterizing transport through 2-D rough-walled fractures; (2) quantifying the relationship between β and 2-D fracture heterogeneities; and (3) quantifying the relationship between solute transport velocity from the CTRW and mean flow velocity from the ADE.

2. Methodology

2.1. High-Resolution Fracture Characterization and Fracture Properties

Here we use the same fracture in *Cardenas et al*. [2007, 2009] where they studied an undisturbed and intact welded Santana tuff sample originating from the Trans-Pecos region of Texas, USA, with an arithmetic mean aperture of 0.63 mm. A total area of 142 cm^2 was scanned at the high-resolution X-ray computed tomography (HRXCT) facility at The University of Texas at Austin. HRXCT measures X-ray attenuation of a fracture sample through a continuous 360° cycle for each vertical increment to get a high-resolution 3-D grid composed of voxels. The approach is described in detail by *Ketcham* and *Carlson* [2001]. In the previous study [*Cardenas et al*., 2007], vertical increment was set at 0.25 mm, while the horizontal field was divided into 512 × 512 voxels with in-plane edge length of 0.23 mm. Fracture aperture and the locations of the top and bottom surfaces were measured to better than 50 μm resolution using methods outlined by *Ketcham et al*. [2010]. As a result, the top and bottom surfaces of the fracture sample consisted of 401 × 603 spatial data points that are used to construct a 3-D digital fracture (Figure 1a). To our knowledge, HRXCT is regarded as the only approach available for determining detailed fracture morphology while the fracture is well preserved and with mated fracture walls [*Ketcham et al*., 2010]. Unlike in *Cardenas et al*. [2007], where they focused on one fracture cross section from the 3-D fracture map, here we used all 2-D cross sections/fractures (∼400) of ∼15 cm length (Figures 1a and 1b) and analyzed them as independent 2-D fractures. Each 2-D fracture is parallel to the red box A–B in Figure 1a with width equal to the horizontal resolution ∼0.23 mm. The 2-D fractures were input into computational fluid dynamics flow and solute transport direct numerical simulations. The method follows and extends the previous study that showed non-Fickian solute transport through one of the 2-D fractures [*Cardenas et al*., 2007].

Previous analysis of the high-resolution data via the roughness-length method showed that the real fracture surfaces are self-affine [*Al-Johar*, 2010], with Hurst exponent estimated to be 0.832 for the top surface and 0.842 for the bottom surface. This Hurst exponent agrees with the common value of 0.8 for natural, self-affine rough surfaces [*Boffa et al*., 1999]. The probability density of the aperture field obeys a log-normal distribution with skewness toward large apertures (Figure 2). The arithmetic mean of apparent aperture $\langle b\rangle$ of individual 2-D fractures ranges from 0.27 to 0.89 mm, the standard deviation σ_b ranges from 0.112 to 1.091 mm, and correlation length λ_b ranges from 1.1 to 105.9 mm (Table 1). The correlation

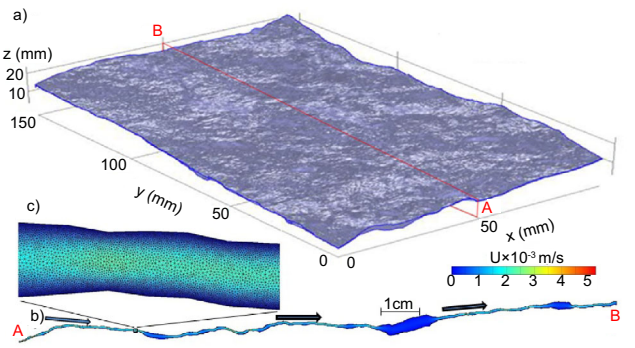

Figure 1. (a) Three-dimensional fracture sample mapped by high-resolution X-ray computed tomography. (b) An example two-dimensional cross section indicated by the red box A–B in Figure 1a used for 2-D simulations; filled color represents magnitude of velocity (U). (c) A magnified section of a portion of Figure 1b to highlight the finite-element mesh.

length is calculated by fitting an exponential model with nugget effect to the experimental semivariogram of the aperture field. The typical exponential semivariogram $\gamma(h)$ model is:

$$\gamma(h) = A\left[1 - exp\left(\frac{h}{\lambda_b}\right)\right] + \gamma_0 \quad (3)$$

where γ_0 is the nugget, A is the sill, h is the lag distance.

2.2. Computational Fluid Dynamics (CFD) Simulation

The CFD model solves the Navier-Stokes and continuity equations which describe single-phase steady flow of an incompressible, isothermal, and homogeneous fluid expressed by:

$$\rho(\boldsymbol{u} \cdot \nabla \boldsymbol{u}) = -\nabla p + \mu \nabla^2 \boldsymbol{u} \quad (4)$$

$$\nabla \cdot \boldsymbol{u} = 0 \quad (5)$$

where $\boldsymbol{u} = [u, w]$ is the velocity vector and p is the total pressure. For the individual 2-D fracture numerical simulations, we assigned fracture surfaces as no-slip boundaries, and applied a given pressure drop $\Delta p = 10$ Pa over the fracture length l (=15 cm) leading to a hydraulic gradient of 0.0068, driving fluid flow from left to right (Figure 1b). Standard fluid properties for water were prescribed: $\rho = 1000$ kg/m^3 and $\mu = 1 \times 10^{-3}$ Pa s. The CFD model was implemented in COMSOL Multiphysics, a generic finite-element model. The fracture domain was discretized into ~90,000 triangular elements. In order to capture the no-slip boundaries accurately, we imposed a finer mesh size (~0.002 mm) near the boundaries and a relatively coarser mesh size (~0.006 mm) at the middle of the domain (Figure 1c). The flow field solved here serves as the basis or input for the direct solute transport simulations.

2.3. Direct Solute Transport Simulation

The advection-diffusion equation describing solute transport through the 2-D fractures is:

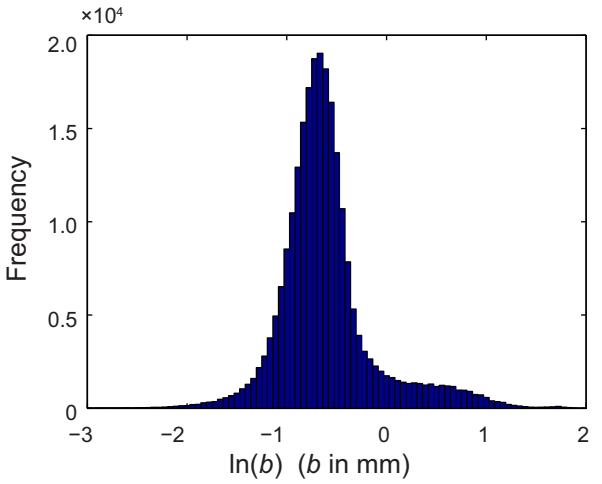

Figure 2. Frequency distribution of logarithm of apparent aperture (b) field for the 3-D fracture showing log-normal distribution with skewness toward large values.

$$\frac{\partial C}{\partial t} = -\nabla(\boldsymbol{u}C) + D_m \nabla^2 C \quad (6)$$

where C is solute concentration, t is time, and D_m is the molecular diffusion coefficient. The solute transport model was also solved with COMSOL Multiphysics. We assumed a typical conservative solute, e.g., Cl^- in water, and set D_m at 2.03×10^{-9} m^2/s [*Li and Gregory*, 1974]. Initial concentration in the fracture domain was:

$$C = 0 \quad 0 < x < l \quad t = 0 \quad (7)$$

while the boundary conditions were specified as:

Table 1. Statistics of 2-D Studied Fractures

Parameter	Symbol	Value
Arithmetic mean	$\langle b \rangle$	0.27–0.89 mm
Standard deviation	σ_b	0.112–1.091 mm
Correlation length	λ_b	1.1–105.9 mm
Reynolds number	*Re*	0.001–0.690
Peclet number	*Pe*	0.79–474.68

$$C = C_0 = 1 \quad x = 0 \quad t \geq 0 \tag{8}$$

$$\partial C / \partial n = 0 \quad x = l \quad 0 \leq t \leq \infty \tag{9}$$

where n represents the normal direction to the outlet boundary. The inlet was a Dirichlet boundary assuming step injection with $C_0 = 1$, whereas the outlet was an open boundary.

Solving equations (6–9) yields the resident concentration time series, from which we can estimate the effluent solute mass by integrating the product of fluid velocity and concentration over the outlet boundary. The 2-D flux-weighted BTCs (C_f) can thus be calculated through a ratio of effluent solute mass to fluid mass, which is:

$$C_f = \frac{\int_0^b uCdz}{\int_0^b udz} \tag{10}$$

We then normalized flux-weighted BTCs and time following:

$$C' = \frac{C_f}{C_0} \tag{11}$$

$$t' = \frac{Qt}{A} \tag{12}$$

where C' is the normalized concentration, t' is the so-called pore volume, Q is the flow rate per length, and A is the area of the fracture. The numerical transport model domain typically had the same ~90,000 elements as the CFD models. Sensitivity analysis to mesh size and time step showed trivial numerical dispersion and that the solutions are mesh-independent.

2.4. Taylor Dispersion Theory

Taylor dispersion is often referred to as shear flow dispersion because it is caused by a stratified velocity field [*Taylor*, 1953]. Taylor dispersion is appropriate for describing solute transport only after some asymptotic time/length scale, at which the longitudinal advective flux is balanced out by in-plane transverse diffusive flux [*Wang et al*., 2012]. The classic Taylor dispersion theory also assumes that there is no additional out-of-plane mixing, i.e., the channel is well mixed in the out-of-plane direction. For transport through parallel plates where the fluid follows Poiseuille (stratified) flow, the Taylor dispersion coefficient (D_{Taylor}) is:

$$D_{\text{Taylor}} = \frac{(\langle u \rangle \langle b \rangle)^2}{210 D_m} = \frac{Q^2}{210 D_m} \tag{13}$$

where Q is simply the product of $\langle u \rangle$ and $\langle b \rangle$ (Tables 1 and 2). Therefore, we can estimate D_{Taylor} based on Q and D_m without conducting direct solute transport simulations.

Table 2. Range of Fitted Parameters and Their Relevant Errors for the ADE and TPL Model Fits to the 2-D Flux-Weighted Breakthrough Curves

ADE			TPL					
$U_{\text{ADE}} \times 10^{-3}$ (m/s)	$D_{\text{ADE}} \times 10^{-6}$ (m^2/s)	E_{ADE}	t_1 (s)	t_2 (s)	β	$U_{\text{TPL}} \times 10^{-3}$ (m/s)	$D_{\text{TPL}} \times 10^{-6}$ (m^2/s)	E_{TPL}
2.14×10^{-3} to 1	2.75×10^{-3} to 2.72	0.03–0.74	$10^{-9.79}$ to $10^{1.01}$	$10^{0.97}$ to $10^{5.45}$	0.94–2.86	6.60×10^{-3} to 35.19	1.42×10^{-3} to 7.73	0.01–0.36

2.5. Continuous Time Random Walk

The general formulation of the CTRW is the Fokker-Planck with memory equation (FPME) [*Berkowitz et al*., 2006; *Cortis and Berkowitz*, 2005; *Cortis et al*., 2004; *Jiménez-Hornero et al*., 2005]. The FPME describing concentration dynamics in a Laplace-transformed one-dimensional (1-D) space is given by:

$$p\tilde{C}(x,p)-C_0(x) = -\tilde{M}(p)\left[U_{\mathrm{TPL}}\frac{\partial}{\partial x}\tilde{C}(x,p)-D_{\mathrm{TPL}}\frac{\partial^2}{\partial x^2}\tilde{C}(x,p)\right] \tag{14}$$

where the tilde represents a variable or function in the Laplace space, the memory function $\tilde{M}(p) = \bar{t}p\frac{\tilde{\psi}(p)}{1-\tilde{\psi}(p)}$ represents how the CTRW captures or represents non-Fickian transport induced by local heterogeneity or processes, p is the Laplace variable, $\tilde{\psi}(p)$ is the transition rate probability, U_{TPL} and D_{TPL} are transport velocity and dispersion coefficient in the context of the CTRW, respectively, which differ from the definitions of mean flow velocity (U_{ADE}) and dispersion coefficient (D_{ADE}) in the context of the ADE [*Berkowitz et al*., 2006]. For the classical ADE derived from mass conservation at continuum scale, U_{ADE} is the temporal rate of change of the first moment of solute concentration, and D_{ADE} is the second central moment of the concentration distribution. We assume that U_{ADE} and D_{ADE} are constant over time and space, i.e., the asymptotic regime, and thus neglecting any variability of the U_{ADE} and D_{ADE} caused by local fracture heterogeneity. However, the U_{TPL} and D_{TPL} in the TPL-CTRW model are not the same as U_{ADE} and D_{ADE} in the ADE. The CTRW is originally derived from mass conservation at the molecular scale through integrating particle transitions over a certain time period [*Berkowitz et al*., 2006]. The specified time period distinguishes the resolved from unresolved scales. The particle movements at unresolved scales are simulated by a probabilistic approach that employs temporal probability density functions (PDFs). The PDF is dependent on the local velocity and molecular diffusion, but variations in the form of the PDFs are largely attributed to the spectrum of possible local velocity fields. Since particle transitions are highly related to the temporal PDF, the U_{TPL} and D_{TPL} are thus correlated to the local velocity variations imposed by local heterogeneities; that is U_{TPL} and D_{TPL} vary over time and space.

The heart of the CTRW model resides in the choice of PDF or transition rate probability $\tilde{\psi}(p)$ to calculate the memory equation. *Cortis et al*. [2004] proposed three possible formulae for $\tilde{\psi}(p)$ to capture non-Fickian transport, including: the asymptotic model, the truncated power law model, and the modified exponential model. Since the TPL is capable of capturing features characterized by the asymptotic model by specifying a large number for the "cutoff time," and since the modified exponential model is designed for diffusion in a random molecular system, we only employed the TPL model.

The formulation of $\tilde{\psi}(p)$ following the TPL model is described by:

$$\tilde{\psi}(p) = (1+\tau_2 p t_1)^{\beta}\exp(t_1 p)\frac{\Gamma(-\beta,\tau_2^{-1}+t_1 p)}{\Gamma(-\beta,\tau_2^{-1})} \tag{15}$$

where t_1 is the time for the onset of the power law, t_2 is cutoff time corresponding to when large-scale Fickian behavior begins or dominates, $\tau_2 = t_2/t_1$, and $\Gamma()$ is the incomplete Gamma function.

2.6. Inverse Modeling Using Breakthrough Curves

Inverse estimation of parameters used in the ADE and the TPL was implemented through the 1-D inverse modeling module of the CTRW Toolbox [*Cortis and Berkowitz*, 2005]. The initial and boundary conditions are similar to the 2-D direct solute transport simulations described in section 2.3. However, inaccurate initial guesses for the parameters would result in convergence to a local minimum error between the 1-D model and the 2-D flux-weighted BTCs resulting from the direct numerical simulations. To avoid this, we iteratively adjusted the initial guesses of parameters until a global minimum error is obtained. The resultant error (E) is used here as the metric for quantifying the goodness-of-fit, which is defined by:

$$E_i = \sqrt{\sum_1^N (C_{1D}^i - C_{2D})^2} \tag{16}$$

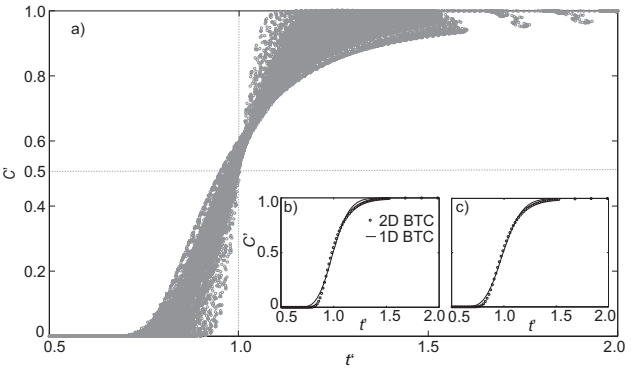

Figure 3. (a) Ensemble of flux-weighted breakthrough curves from 2-D direct solute transport simulations showing ubiquitous non-Fickian behavior. The inverse estimation of the dispersion coefficient using the advection-dispersion equation (ADE) model shows the degree to which the 1-D ADE model misses the arrival and tails of the 2-D BTCs; this depends on the fracture heterogeneity as indicated in inset plots, (b) $\sigma_b/\langle b\rangle = 0.80$, and (c) $\sigma_b/\langle b\rangle = 0.69$. b is the apparent aperture with standard deviation σ_b and arithmetic mean $\langle b\rangle$.

where N is the number of data points in the BTCs, C^i_{1D} constitute the 1-D BTCs fitted using the ADE and TPL models, where i signifies either the ADE or the TPL, and C_{2D} constitute the flux-weighted, spatially integrated BTCs. Errors from the ADE and TPL models are denoted as E_{ADE} and E_{TPL}, respectively.

For the inverse modeling with the ADE, the initial guesses for the fitted parameters, including velocity U_{ADE} and dispersion coefficient D_{ADE}, were based on the Cubic Law and the Taylor dispersion theory, respectively. The non-Fickian transport inverse modeling used the following free parameters for the TPL model: t_1 and t_2, β, U_{TPL}, and D_{TPL}. Initial estimates of U_{TPL} and D_{TPL} took on the values from the ADE inverse modeling. Moreover, since the TPL is most sensitive to β while relatively insensitive to the time scale $t_1$and t_2 [*Cortis and Berkowitz*, 2005], we chose a broad range for β, from 0.8 to 2, whereas initial guesses for t_1 and t_2 were almost constant.

3. Results

3.1. Non-Fickian Transport Behavior

The typical non-Fickian transport behavior of early arrivals and heavy tails were observed in most of the BTCs from 2-D direct solute transport simulations (Figures 3b and 3c). The presence and growth of eddies in rough-walled fractures could lead to non-Fickian transport behavior [*Cardenas et al.*, 2007]. But here, we find that non-Fickian transport is ubiquitous with or without the presence of eddies (Figure 3a) and probably due mainly to advection through a tortuous fracture [*Becker and Shapiro*, 2000]. All of the flux-weighted BTCs converged to a unique dimensionless concentration $C' \sim 0.6$ at dimensionless time $t' \sim 1$. All these show early breakthrough since in Fickian transport $C' \sim 0.5$ at $t' \sim 1$.

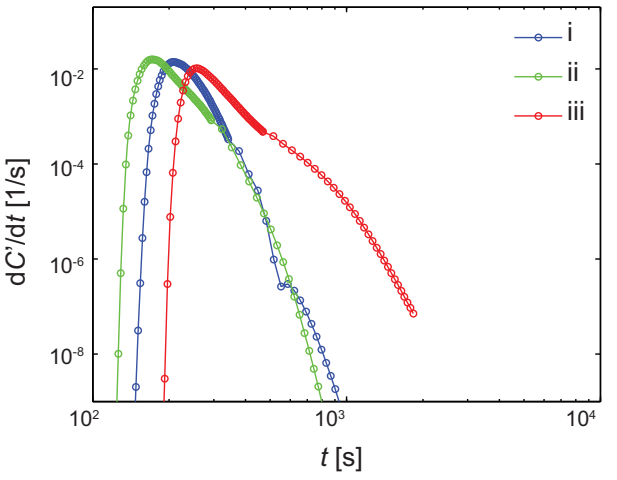

Figure 4. Examples of different forms of residence time distributions showing ubiquitous occurrence of non-Fickian transport behavior through 2-D rough-walled fractures including: (i) a narrow shoulder after the peak, (ii) a heavy tail, and (iii) deviation from Gaussian distribution after the peak.

The time derivative of 2-D flux-weighted BTCs for step injection results in the residence time distribution (RTD). Power law tails in the RTDs, another typical characteristic of non-Fickian transport, were observed. Figure 4 displays some different types of RTDs for various fracture heterogeneities illustrating that variations in fracture geometry could lead to different power law tails; this has also been shown previously [*Cardenas et al.*, 2009].

3.2. Validity of the Taylor Dispersion Theory to Estimate Dispersion Coefficient D_{ADE}

The fitted U_{ADE} and D_{ADE} and the corresponding errors for the ADE

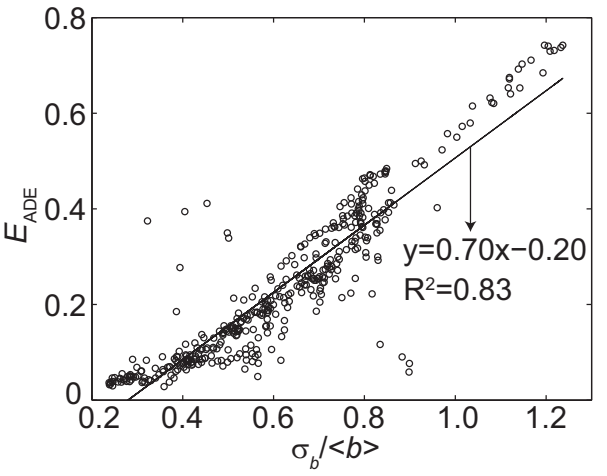

Figure 5. Errors associated with fitting breakthrough curves using the advection-dispersion equation (E_{ADE}). The error increases linearly with heterogeneity $\sigma_b/\langle b\rangle$, where b is apparent aperture with standard deviation of aperture σ_b and arithmetic mean aperture $\langle b\rangle$.

model are shown in Table 2. The subtle difference in BTCs fitted by the 1-D ADE model and from the 2-D direct solute transport simulations is quantified through equation (16), and can be interpreted as a metric for the appropriateness of approximating a potentially non-Fickian transport phenomenon with a Fickian transport model (Figure 5). The values of E_{ADE} for 2-D fractures range from 0.03 to 0.74, with higher values corresponding to increasing heterogeneity, i.e., $\sigma_b/\langle b\rangle$, directly showing that the ADE model with constant D_{ADE} becomes less accurate for rougher fractures.

The D_{ADE} values follow a quasi-normal distribution with skewness toward small values (Figure 6). To test the accuracy of Taylor dispersion theory in approximating D_{ADE}, we compare the ratio of D_{ADE} to D_{Taylor} with heterogeneity. The ratio is proportional to the heterogeneity (Figure 7) and ranges from 1 to 5 suggesting that assuming Taylor dispersion (suitable for parallel plates) while neglecting the effect of heterogeneity on solute transport, will underestimate the mixing and spreading processes, with underestimation becoming worse with increasing fracture heterogeneity. Additionally, Figure 7 gives the impression that when $\sigma_b/\langle b\rangle < 0.5$ (and when $Pe < 500$ at Table 1), Taylor dispersion theory is sufficient for predicting D_{ADE}. However, additional simulations with increasing Pe for the same fractures showed that the Taylor dispersion theory initially underestimates D_{ADE} at lower Pe, then overestimates D_{ADE} at higher Pe (Figure 8a). Therefore, the 2-D cases we investigated suggest that it may be inappropriate to only use Taylor dispersion theory to predict D_{ADE} even at high Pe when it has been shown to perform well for vertically integrated 3-D fractures [*Detwiler et al*., 2000].

Substitution of equation (1) into equation (13) yields:

$$\frac{D_{Taylor}}{D_m} = \frac{Pe^2}{210} \tag{17}$$

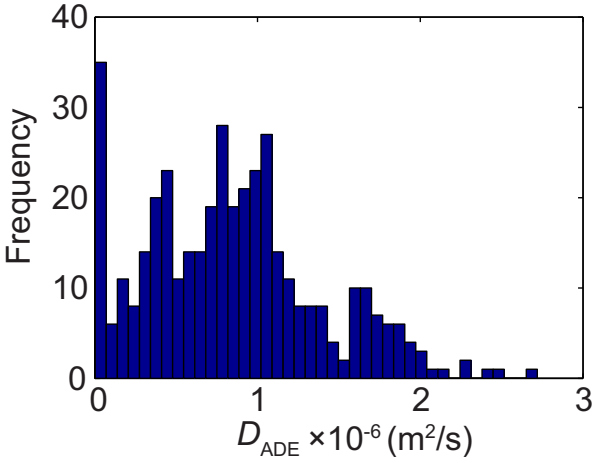

Figure 6. Frequency distribution of fitted dispersion coefficient (D_{ADE}).

which shows that the D_{Taylor}/D_m has a power law relationship with Pe with an exponent equal to 2 [*Detwiler et al*., 2000]. However, in the case of our numerical simulation results, the exponent is always less than 2, and is inversely linearly related to $\sigma_b/\langle b\rangle$ for the studied fractures (Figures 8b and 9).

3.3. Performance of the TPL in Characterizing Non-Fickian Transport Behavior

The errors from fitting the TPL model to 2-D direct transport simulation results are shown in Figures 10a, 10b, and Table 2. The ratios of E_{TPL} to E_{ADE}, which ranged

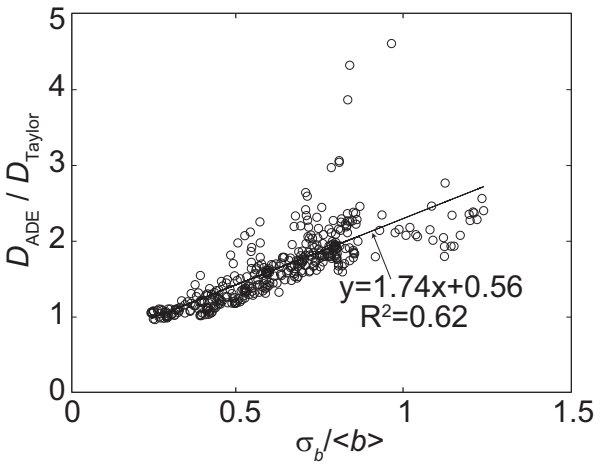

Figure 7. The deviation of D_{Taylor} from D_{ADE} is linearly dependent on heterogeneity $\sigma_b/\langle b\rangle$ for cases where Peclet number <500. b is the apparent aperture with standard deviation σ_b and arithmetic mean $\langle b\rangle$.

from 0.04 to 0.95, were all less than 1 for the ensemble of 2-D fractures. Thus, and not surprisingly, the TPL performs substantially better than the ADE for characterizing non-Fickian transport. Furthermore, the ratios decrease fairly linearly with $\sigma_b/\langle b\rangle$, showing that fracture heterogeneity has a pronounced impact on the non-Fickian transport behavior.

We further plotted β against heterogeneity to find any inherent relationship between them. As expected, β decreased linearly from $\sim$2 to $\sim$1 with increasing $\sigma_b/\langle b\rangle$ (Figure 11). This illustrates that the transition from non-Fickian to Fickian transport depends on the degree of heterogeneity. However, the cases where effective Peclet number ($Pe_{eff} = \langle u\rangle\langle b\rangle/D_{ADE}$) > 1 were excluded from this analysis. This is because advection-dominated transport tends to follow Fickian behavior [*Detwiler et al*., 2000], where the β is expected to be $\geq$2; in fact, majority of these cases complied with this assumption (Figure 11). Consequently, these cases are irrelevant for the purpose of quantifying non-Fickian transport in terms of β since they are a fraction of all cases.

4. Discussion

4.1. Inappropriate Estimation of D_{ADE} Based on the Taylor Dispersion Theory

Molecular diffusion, Taylor dispersion, and macrodispersion constitute the complete Fickian dispersion mechanism through fractures [*Detwiler et al*., 2000]. D_{Taylor} is always smaller than D_{ADE}, with the difference dependent on the fracture heterogeneity when $Pe < 500$ for the studied cases (Figure 7). This further and clearly illustrates that heterogeneity plays a significant role in facilitating the mixing and spreading processes by forcing fluid flow through low-aperture regions of 2-D rough-walled fractures. The Taylor dispersion theory is therefore inappropriate for estimating solute mixing and spreading in rough-walled fractures at relatively low Pe regime.

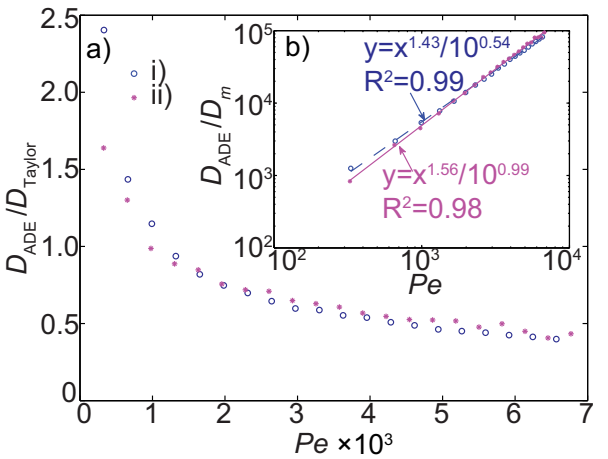

Figure 8. (a) The Taylor dispersion coefficient (D_{Taylor}) is either smaller or greater than D_{ADE} with increasing Peclet number (Pe), indicating that Taylor dispersion theory is invalid for both cases where heterogeneities are (i) $\sigma_b/\langle b\rangle = 1.24$ and (ii) $\sigma_b/\langle b\rangle = 0.41$. Inset (b) different exponents for the power law relationship between Pe and the ratio of D_{ADE} to the molecular diffusion coefficient D_m. b is the apparent aperture with standard deviation σ_b and arithmetic mean $\langle b\rangle$.

Numerous efforts have shown that Taylor dispersion theory is expected to be valid where Pe is relatively high so as 3-D macrodispersion can be neglected [e.g., *Roux et al*., 1998; *Detwiler et al*., 2000]. However, our numerical experimental results show otherwise for 2-D fractures. As Pe increases, D_{Taylor} may either underestimate ($Pe < \sim$1000) or

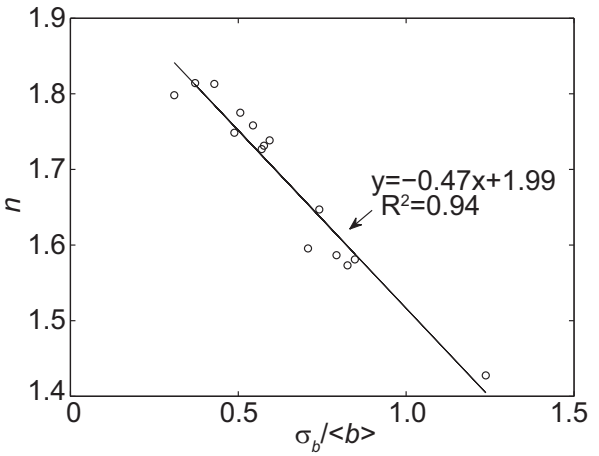

Figure 9. Dependence of power law exponent (n; the exponent in the scaling relationship of D_{ADE}/D_m to Peclet number) on heterogeneity $\sigma_b/\langle b\rangle$ for different fractures. The exponents are determined by fitting $y = ax^n$, as illustrated in Figure 8b. b is the apparent aperture with standard deviation σ_b and arithmetic mean $\langle b\rangle$.

overestimate ($Pe > \sim 1000$) D_{ADE} (Figure 8). Moreover, our results do not obey the previous power law scaling with an exponent of 2 previously proposed for D_{Taylor}'s dependence on Pe for vertically integrated 3-D fractures [*Detwiler et al*., 2000]. For our 2-D vertical plane cases, the exponent deviates from 2 with increasing heterogeneity via an inverse linear relationship (Figure 9). The difference is likely and partly due to the fact that the previous study relied on flow fields generated by the Reynolds lubrication equation which does not consider the interacting effects of heterogeneity and inertia. That is, previous studies did not fully capture the complexity inherent in inertial flow and transport in rough single fractures across a range of Peclet and Reynolds numbers. On the other hand, our 2-D examples negate preferential flow and out-of-plane transverse diffusive/dispersive process, which are present in the cases studied by *Detwiler et al*. [2000]. The absence of out-plane diffusive/dispersive flux makes it less likely that the longitudinal solute advective flux is balanced out, since only in-plane transverse diffusive/dispersive process occurs in our 2-D cases; this balance of fluxes is a critical assumption in the Taylor dispersion theory, and further explains why our 2-D results are different from that for 3-D fractures.

4.2. Dependence of Non-Fickian Transport Magnitude on Heterogeneity

Rough surfaces acting as no-slip walls lead to classic "parabolic" flow profiles but in a complex way. This may lead to non-Fickian solute transport (Figures 3 and 4). Our attempts to quantify non-Fickian transport through a Fickian model with D_{ADE} reveal that the degree of non-Fickian behavior, i.e., the resultant fitting errors, is linearly dependent on the fracture heterogeneity (Figure 5). Furthermore, the increasing discrepancy between D_{ADE} and D_{Taylor} when plotted against heterogeneity supports this (Figure 7). It has been previously shown through direct numerical simulations that eddies (or stagnation zones) cause non-Fickian transport [*Cardenas et al*., 2007]. While early breakthrough of the solute followed by power law tailing is prevalent in our numerical experiments, only a portion of the fractures we considered likely host large eddies, however.

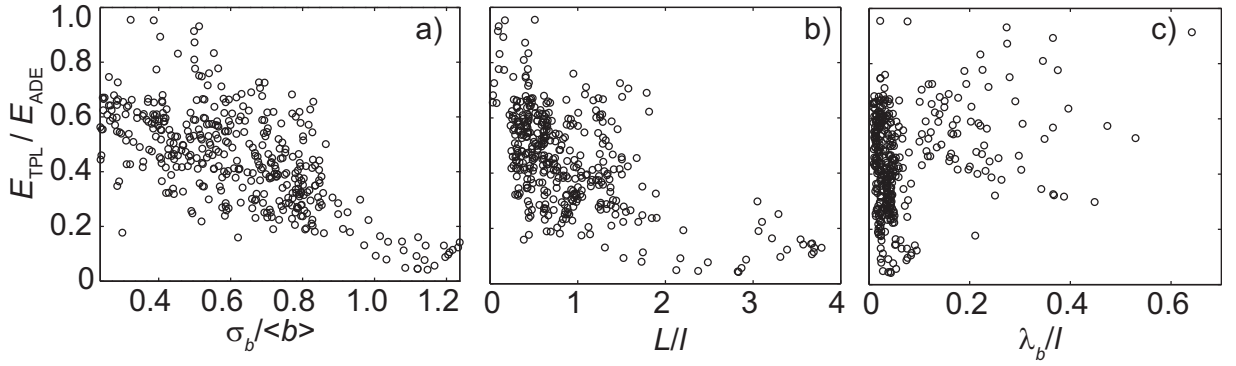

Figure 10. The ratios of error in breakthrough curve fitting using the TPL to that using the ADE. E_{TPL} and E_{ADE} are errors defined in the equation (16) from the TPL and ADE models. The ratios: (a) decrease with heterogeneity $\sigma_b/\langle b\rangle$, where b is the apparent aperture with standard deviation σ_b and arithmetic mean $\langle b\rangle$, (b) decrease with dimensionless length L/l, where L is asymptotic length scales calculated through equation (31) in *Wang et al*. [2012] and l is the fracture length (~15 cm), and (c) are independent of correlation length ratio λ_b/l, where λ_b is correlation length.

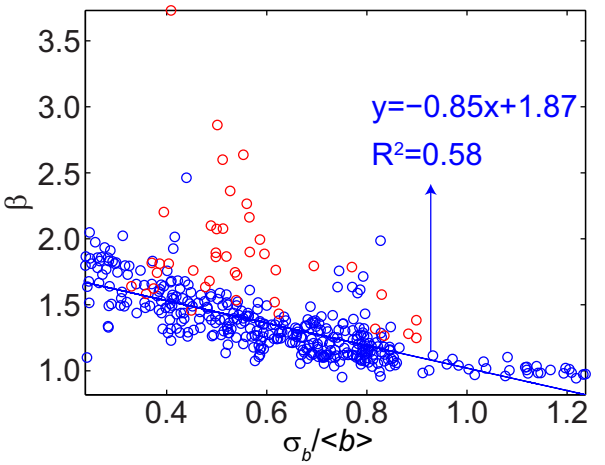

Figure 11. Dependence of parameter β in the TPL model on heterogeneity $\sigma_b/\langle b\rangle$, where b is apparent aperture with standard deviation of aperture σ_b and arithmetic mean aperture $\langle b\rangle$. Blue circles are those whose effective Peclet number ($Pe_{\text{eff}} = \langle u\rangle\langle b\rangle/D_{\text{ADE}}$) <= 1 and red circles with $Pe_{\text{eff}} > 1$, where $\langle u\rangle$ is mean flow velocity, D_{ADE} is fitted dispersion coefficient through 1-D ADE model. Blue line represents the linear regression of β with heterogeneity based only on the blue circles.

Non-Fickian behavior could also be caused by a spreading process that would not reach its asymptotic value if the time and length scales over which solute transport occurs are the same order of the variation in velocity field [*Koch and Brady*, 1987]. To this end, we calculated the potential length scales (L) that separate Fickian and non-Fickian transport. The calculation is based on the model for equivalent parallel plates following equation (31) in *Wang et al.* [2012]. We found that L ranges from 4.76×10^{-3} m to 0.57 m with 29% of L greater than the studied fracture length ($l \sim 0.15$ m). Additionally, the ratios of error $E_{\text{TPL}}/E_{\text{ADE}}$ decrease with dimensionless length L/l (Figure 10b), demonstrating that as L/l becomes >1 non-Fickian transport tends to be more pronounced since the fracture length falls short of its asymptotic dispersion threshold. This has also been observed for solute transport through pores [*Cardenas*, 2009]. Since some of our numerical experiments cover preasymptotic space (or time) a time-dependent dispersion coefficient would be appropriate for the ADE [*Dentz and Carrera*, 2007; *Wang et al*., 2012]. Nonetheless, it is clear that that the cases we considered are better represented by non-Fickian transport models.

Modeling non-Fickian transport through the TPL-CTRW model which allows for the unresolved local heterogeneity notably improved the BTC fits (Figure 10a). The TPL model embedded in the CTRW is capable of capturing the early arrival and power law tailing phenomenon while the ADE falls short. This is due to the fact that the TPL-CTRW has more flexible fitting parameters than the ADE does, which makes the TPL-CTRW mathematically easier to optimize to the 2-D flux-weighted BTCs. Physically, this is because the ADE inherently treats heterogeneous fractures as homogeneous media where flow velocity and dispersion coefficient are constant in space and time. On the other hand, the CTRW model uses a transition probability function allowing for local heterogeneity; this more accurately models the actual solute transport dynamics. In fact, the TPL-CTRW model performs better than the standard ADE even when the fracture length scale is above the calculated asymptotic scale, i.e., $L/l < 1$ (Figure 10b). This highlights the importance and contribution of fracture heterogeneity toward non-Fickian transport at the asymptotic dispersion regime.

The correlation length of the aperture field contributes little to non-Fickian behavior in our studied 2-D fractures (Figure 10c). The ratios of error E_{TPL}/E_{ADE} are independent of correlation length. This shows that the transport process through 3-D fractures are different to 2-D fractures, where non-Fickian behavior is nonetheless still prevalent. This might be caused by the fact that the correlation length is not much shorter than the computational domain length. Consequently, the highly conductive zones in 3-D fractures are more likely to be connected, and provides preferential/channelized flow paths which promote non-Fickian behavior. However, fluid flow through 2-D fractures does not have these preferential flow paths, which are best described by the correlation length, and thus the effect of correlation length on solute transport is not as critical as it is for 3-D fractures.

Another metric for the degree of non-Fickian transport is β, which we show is proportional to the fracture heterogeneity (Figure 11). The effective dispersion coefficient Pe_{eff} to some extent determines the propensity for non-Fickian transport [*Detwiler et al*., 2000]; however, we neglect its effects since Pe_{eff} is generally small ($Pe_{\text{eff}} < 2.5$) in our simulations. This assumption is probably responsible for fluctuations of β around the regression line (Figure 11). That is, some of the variation is inherently due to the relative importance of advective and dispersive transport processes. Most values of β range from 1 to 2 representing the

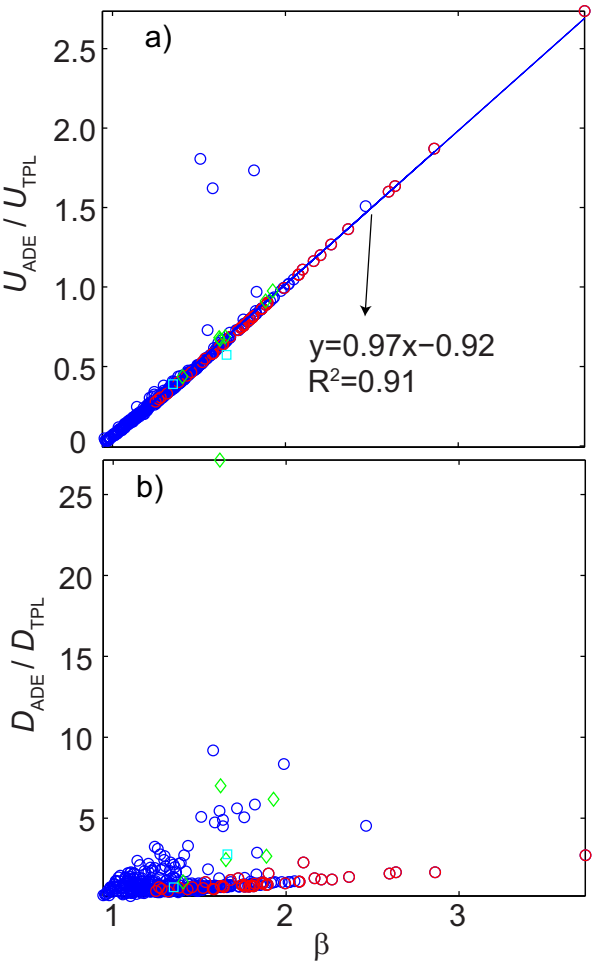

Figure 12. The ratios of pertinent velocities (U) and dispersion coefficients (D) estimated inversely using the ADE and using the TPL plotted against β. Blue circles (effective Peclet number $Pe_{eff} <= 1$) and red circles ($Pe_{eff} > 1$) are results of this study, green diamonds are from *Jimenez-Hornero et al*. [2005], and cyan squares are from *Nowamooz et al*. [2013]. (a) Velocity ratio increases linearly with β; (b) dispersion coefficient ratio exhibits no systematic relationship with β.

moderate non-Fickian transport regime where CTRW transport velocity is constant over time while the dispersion coefficient scales following a power law [*Dentz et al*., 2004]. The connection between β and heterogeneity which we established allows for upscaling the effects of local spreading and mixing processes within the CTRW framework, at least for 2-D fractures. That is, β, which is an effective property, can be predicted from mapped b fields.

4.3. Dependence of the Ratio of Mean Flow Velocity to CTRW Transport Velocity on β

Even though the inverse modeling with the TPL-CTRW model is relatively insensitive to the parameters U_{TPL}, D_{TPL}, t_1, and t_2 compared to β, the identification of U_{TPL}, D_{TPL} is also crucial for understanding and therefore predicting non-Fickian transport. This is particularly true for U_{TPL} [*Nowamooz et al*., 2013]. To this end, we compared U_{TPL} and D_{TPL} to U_{ADE} and D_{ADE} (Table 2). In addition to the inverse modeling results of this study, we further considered associated results from previous studies which used the TPL model to characterize non-Fickian transport through 3-D rough-walled fractures [*Jiménez-Hornero et al*., 2005; *Nowamooz et al*., 2013]. Figure 12a demonstrates that the velocity ratio, i.e., U_{ADE}/U_{TPL}, is linearly proportional to β with a slope close to 1. Moreover, since β is linearly dependent on the heterogeneity when $Pe_{eff} < 1$(Figure 11), we can thus infer that the velocity ratio is proportional to heterogeneity as well. The deviation of transport velocity from mean flow velocity in fractures could be due to local velocity variability resulting from fracture heterogeneity. For example, a preferential flow path would case the transport velocity to be greater than mean fluid velocity, and this will be responsible for fast solute arrival. On the other hand, eddy growth in 2-D fractures would retard transport velocity and lead to heavy tails [*Cardenas et al*., 2007]. However, the ratio D_{ADE}/D_{TPL} did not show a systematic relationship with β (Figure 12b). This is partly due to the fact that by taking into account a transition rate function, the D_{TPL} scales with time following a power law at moderate non-Fickian transport regimes ($1 < \beta < 2$) [*Berkowitz et al*., 2006], while the D_{ADE} does not consider local transport effects and is temporally constant. The results here show that one could conceivably predict transport velocity for the TPL-CTRW model based on mean flow velocity and heterogeneity.

5. Summary and Conclusion

We conducted direct numerical simulations of solute transport using 2-D maps extracted from a real fracture. Breakthrough curves from the simulations show non-Fickian behavior with early arrival followed by

power law tailing. The results show that the Taylor dispersion theory may be insufficient for reproducing the breakthrough curves even at high Peclet numbers. The degree of non-Fickian transport was shown to depend on fracture heterogeneity. Accurate analysis of non-Fickian transport was implemented using inversely estimated parameters through the continuous time random walk model with a truncated power law transition probability for consideration of the unresolved local heterogeneity. For the moderate non-Fickian transport, where $1 < \beta < 2$ for the truncated power law, β was found to be linearly proportional to fracture heterogeneity. In addition, the ratio of mean flow velocity (within the context of the standard advection-dispersion equation) to CTRW transport velocity (within the context of continuous time random walk) is proportional to β. However, no relationship was observed that would allow for prediction of the dispersion coefficient within the context of continuous time random walk. Our study now allows for prediction of transport with the continuous time random walk model based on measurable physical properties. However, this potentially predictive capability needs to be extended and tested first using more fractures, and with the consideration for three-dimensional cases which naturally allows for anisotropy.

Acknowledgments

This material is based upon work supported as part of the Center for Frontiers of Subsurface Energy Security (CFSES) at the University of Texas at Austin, an Energy Frontier Research Center funded by the U.S. Department of Energy, Office of Science, Office of Basic Energy Sciences under Award DE-SC0001114. Additional support was provided by the Geology Foundation of the University of Texas. We thank colleagues at the University of Texas—Donald Slottke, Richard Ketcham, and Jack Sharp—for sharing the fracture data. We thank Associate Editor Xavier Sanchez-Vila and three anonymous reviewers for their insightful comments in evaluating this manuscript.

References

Al-Johar, M. M. (2010), Constraining fracture permeability by characterizing fracture surface roughness, MS thesis, Univ. of Texas at Austin, Austin.

Aris, R. (1956), On the dispersion of a solute in a fluid flowing through a tube, *Proc. R. Soc. London, Ser. A*, *235*(1200), 67–77, doi:10.1098/rspa.1956.0065.

Bauget, F., and M. Fourar (2008), Non-Fickian dispersion in a single fracture, *J. Contam. Hydrol.*, *100*(3–4), 137–148, doi:10.1016/j.jconhyd.2008.06.005.

Becker, M. W., and A. M. Shapiro (2000), Tracer transport in fractured crystalline rock: Evidence of nondiffusive breakthrough tailing, *Water Resour. Res.*, *36*(7), 1677–1686, doi:10.1029/2000WR900080.

Berkowitz, B. (2002), Characterizing flow and transport in fractured geological media: A review, *Adv. Water Resour.*, *25*(8–12), 861–884, doi:10.1016/s0309-1708(02)00042-8.

Berkowitz, B., and H. Scher (1997), Anomalous transport in random fracture networks, *Phys. Rev. Lett.*, *79*(20), 4038–4041, doi:10.1103/PhysRevLett.79.4038.

Berkowitz, B., and H. Scher (1998), Theory of anomalous chemical transport in random fracture networks, *Phys. Rev. E*, *57*(5), 5858–5869, doi:10.1103/PhysRevE.57.5858.

Berkowitz, B., A. Cortis, M. Dentz, and H. Scher (2006), Modeling non-Fickian transport in geological formations as a continuous time random walk, *Rev. Geophys.*, *44*, RG2003, doi:10.1029/2005RG000178.

Boffa, J. M., C. Allain, R. Chertcoff, J. P. Hulin, F. Plouraboué, and S. Roux (1999), Roughness of sandstone fracture surfaces: Profilometry and shadow length investigations, *Eur. Phys. J. B*, *7*(2), 179–182, doi:10.1007/s100510050602.

Cardenas, M. B. (2009), Direct simulation of pore level Fickian dispersion scale for transport through dense cubic packed spheres with vortices, *Geochem. Geophys. Geosyst.*, *10*, Q12014, doi:10.1029/2009GC002593.

Cardenas, M. B., D. T. Slottke, R. A. Ketcham, and J. M. Sharp Jr. (2007), Navier-Stokes flow and transport simulations using real fractures shows heavy tailing due to eddies, *Geophys. Res. Lett.*, *34*, L14404, doi:10.1029/2007GL030545.

Cardenas, M. B., D. T. Slottke, R. A. Ketcham, and J. M. Sharp Jr. (2009), Effects of inertia and directionality on flow and transport in a rough asymmetric fracture, *J. Geophys. Res.*, *114*, B06204, doi:10.1029/2009JB006336.

Chen, Z., J. Qian, H. Zhan, L. Chen, and S. Luo (2010), Mobile-immobile model of solute transport through porous and fractured media, in *Proceedings of ModelCARE 2009*, 274 pp., IAHS Press, Wallingford, U. K.

Cortis, A., and B. Berkowitz (2004), Anomalous transport in classical soil and sand columns, *Soil Sci. Soc. Am. J.*, *68*(5), 1539–1548, doi:10.2136/sssaj2004.1539.

Cortis, A., and B. Berkowitz (2005), Computing "anomalous" contaminant transport in porous media: The CTRW MATLAB Toolbox, *Ground Water*, *43*(6), 947–950, doi:10.1111/j.1745-6584.2005.00045.x.

Cortis, A., C. Gallo, H. Scher, and B. Berkowitz (2004), Numerical simulation of non-Fickian transport in geological formations with multiple-scale heterogeneities, *Water Resour. Res.*, *40*, W04209, doi:10.1029/2003WR002750.

Cvetkovic, V., S. Painter, N. Outters, and J. O. Selroos (2004), Stochastic simulation of radionuclide migration in discretely fractured rock near the Äspö Hard Rock Laboratory, *Water Resour. Res.*, *40*, W02404, doi:10.1029/2003WR002655.

Dentz, M., and J. Carrera (2007), Mixing and spreading in stratified flow, *Phys. Fluids*, *19*(1), 017107–017117, doi:10.1063/1.2427089.

Dentz, M., A. Cortis, H. Scher, and B. Berkowitz (2004), Time behavior of solute transport in heterogeneous media: Transition from anomalous to normal transport, *Adv. Water Resour.*, *27*(2), 155–173, doi:10.1016/j.advwatres.2003.11.002.

Detwiler, R. L., H. Rajaram, and R. J. Glass (2000), Solute transport in variable-aperture fractures: An investigation of the relative importance of Taylor dispersion and macrodispersion, *Water Resour. Res.*, *36*(7), 1611–1625, doi:10.1029/2000WR900036.

Gelhar, L. W., and C. L. Axness (1983), Three-dimensional stochastic analysis of macrodispersion in aquifers, *Water Resour. Res.*, *19*(1), 161–180, doi:10.1029/WR019i001p00161.

Gelhar, L. W., C. Welty, and K. R. Rehfeldt (1992), A critical review of data on field-scale dispersion in aquifers, *Water Resour. Res.*, *28*(7), 1955–1974, doi:10.1029/92WR00607.

Haggerty, R. (2013), Analytical solution and simplified analysis of coupled parent-daughter steady-state transport with multirate mass transfer, *Water Resour. Res.*, *49*, 635–639, doi:10.1029/2012wr012821.

Jiménez-Hornero, F. J., J. V. Giráldez, A. Laguna, and Y. Pachepsky (2005), Continuous time random walks for analyzing the transport of a passive tracer in a single fissure, *Water Resour. Res.*, *41*, W04009, doi:10.1029/2004WR003852.

Keller, A. A., P. V. Roberts, and P. K. Kitanidis (1995), Prediction of single phase transport parameters in a variable aperture fracture, *Geophys. Res. Lett.*, *22*(11), 1425–1428, doi:10.1029/95GL01497.

Keller, A. A., P. V. Roberts, and M. J. Blunt (1999), Effect of fracture aperture variations on the dispersion of contaminants, *Water Resour. Res.*, *35*(1), 55–63, doi:10.1029/1998WR900041.

Ketcham, R. A., and W. D. Carlson (2001), Acquisition, optimization and interpretation of X-ray computed tomographic imagery: Applications to the geosciences, *Comput. Geosci.*, *27*(4), 381–400, doi:10.1016/s0098-3004(00)00116-3.
Ketcham, R. A., D. T. Slottke, and J. M. Sharp (2010), Three-dimensional measurement of fractures in heterogeneous materials using high-resolution X-ray computed tomography, *Geosphere*, *6*(5), 499–514, doi:10.1130/ges00552.1.
Koch, D. L., and J. F. Brady (1987), A non-local description of advection-diffusion with application to dispersion in porous media, *J. Fluid Mech.*, *180*, 387–403, doi:10.1017/S0022112087001861.
Li, Y., and S. Gregory (1974), Diffusion of ions in sea water and in deep-sea sediments, *Geochim. Cosmochim. Acta*, *38*(5), 703–714, doi:10.1016/0016-7037(74)90145-8.
Maloszewski, P., and A. Zuber (1990), Mathematical modeling of tracer behavior in short-term experiments in fissured rocks, *Water Resour. Res.*, *26*(7), 1517–1528, doi:10.1029/WR026i007p01517.
Margolin, G., and B. Berkowitz (2004), Continuous time random walks revisited: First passage time and spatial distributions, *Physica A*, *334*(1–2), 46–66, doi:10.1016/j.physa.2003.10.069.
Neuman, S. P. (2005), Trends, prospects and challenges in quantifying flow and transport through fractured rocks, *Hydrogeol. J.*, *13*(1), 124–147, doi:10.1007/s10040-004-0397-2.
Neuman, S. P., and D. M. Tartakovsky (2009), Perspective on theories of non-Fickian transport in heterogeneous media, *Adv. Water Resour.*, *32*(5), 670–680, doi:10.1016/j.advwatres.2008.08.005.
Nowamooz, A., G. Radilla, M. Fourar, and B. Berkowitz (2013), Non-Fickian transport in transparent replicas of rough-walled rock fractures, *Transp. Porous Med.*, *98*(3), 651–682, doi:10.1007/s11242-013-0165-7.
Qian, J., Z. Chen, H. Zhan, and S. Luo (2011), Solute transport in a filled single fracture under non-Darcian flow, *Int. J. Rock Mech. Min. Sci.*, *48*(1), 132–140, doi:10.1016/j.ijrmms.2010.09.009.
Robinson, N. I., J. M. Sharp, and I. Kreisel (1998), Contaminant transport in sets of parallel finite fractures with fracture skins, *J. Contam. Hydrol.*, *31*(1–2), 83–109, doi:10.1016/s0169-7722(97)00055-7.
Roux, S., F. Plouraboué, and J.-P. Hulin (1998), Tracer dispersion in rough open cracks, *Transp. Porous Med.*, *32*(1), 97–116, doi:10.1023/a:1006553902753.
Silliman, S. E., and E. S. Simpson (1987), Laboratory evidence of the scale effect in dispersion of solutes in porous media, *Water Resour. Res.*, *23*(8), 1667–1673, doi:10.1029/WR023i008p01667.
Sudicky, E. A., and E. O. Frind (1982), Contaminant transport in fractured porous media: Analytical solutions for a system of parallel fractures, *Water Resour. Res.*, *18*(6), 1634–1642, doi:10.1029/WR018i006p01634.
Taylor, G. (1953), Dispersion of soluble matter in solvent flowing slowly through a tube, *Proc. R. Soc. London, Ser. A*, *219*(1137), 186–203, doi:10.1098/rspa.1953.0139.
Tsang, Y. W. (1984), The effect of tortuosity on fluid flow through a single fracture, *Water Resour. Res.*, *20*(9), 1209–1215, doi:10.1029/WR020i009p01209.
Tsang, Y. W., and C. F. Tsang (1989), Flow channeling in a single fracture as a two-dimensional strongly heterogeneous permeable medium, *Water Resour. Res.*, *25*(9), 2076–2080, doi:10.1029/WR025i009p02076.
Wang, P., C. Zheng, and S. M. Gorelick (2005), A general approach to advective–dispersive transport with multirate mass transfer, *Adv. Water Resour.*, *28*(1), 33–42, doi:10.1016/j.advwatres.2004.10.003.
Wang, L., M. B. Cardenas, W. Deng, and P. C. Bennett (2012), Theory for dynamic longitudinal dispersion in fractures and rivers with Poiseuille flow, *Geophys. Res. Lett.*, *39*, L05401, doi:10.1029/2011GL050831.
Zheng, Q., S. Dickson, and Y. Guo (2009), Influence of aperture field heterogeneity and anisotropy on dispersion regimes and dispersivity in single fractures, *J. Geophys. Res.*, *114*, B03205, doi:10.1029/2007JB005161.
Zhou, Q., H.-H. Liu, G. Bodvarsson, and F. Molz (2006), Evidence of multi-mrocess matrix diffusion in a single fracture from a field tracer test, *Transp. Porous Med.*, *63*(3), 473–487, doi:10.1007/s11242-005-1123-9.